



Open Research Online

The Open University's repository of research publications and other research outputs

Effect of prior cold work on the mechanical properties of weldments

Conference or Workshop Item

How to cite:

Acar, Murat; Gungor, Salih; Bouchard, Peter and Fitzpatrick, M. E. (2010). Effect of prior cold work on the mechanical properties of weldments. In: Proceedings of the 2010 SEM Annual Conference and Exposition on Experimental and Applied Mechanics, 7-10 Jun 2010, Indianapolis, Indiana, USA.

For guidance on citations see [FAQs](#).

© 2010 Society for Experimental Mechanics Inc.

Version: Accepted Manuscript

Copyright and Moral Rights for the articles on this site are retained by the individual authors and/or other copyright owners. For more information on Open Research Online's [data policy](#) on reuse of materials please consult the policies page.

oro.open.ac.uk

Effect of Prior Cold Work on the Mechanical Properties of Weldments

M. Acar*, S. Gungor, P. J. Bouchard and M. E. Fitzpatrick

Materials Engineering
The Open University, Walton Hall
Milton Keynes MK7 6AA, UK

*Corresponding author: m.o.acar@open.ac.uk

ABSTRACT

Heat exchanger units used in steam raising power plant are often manufactured using many metres of austenitic stainless steel tubes that have been plastically formed (bent and swaged) and welded into complex shapes. The amount of plastic deformation (pre-straining) before welding varies greatly. This has a significant effect on the mechanical properties of the welded tubes and on the final residual stress state after welding. The aim of the present work was to measure and understand the combined effects of pre-straining and welding on the properties and residual stress levels in stainless steel tubing weldments. Effects of plastic deformation were simulated by plastically straining three identical stainless steel tubes to different strain levels (0%, 10% and 20%). Then each tube was cut into two halves and welded back together. The variation in mechanical properties across weldments was measured using digital image correlation (DIC) and a series of strain gauges (SG). Residual stresses were measured on the 0% (undeformed) and 20% prestrained and welded tubes by neutron diffraction. It was found that the welding process had a marked effect on the tensile properties of parent material within 25mm of the weld centre-line. Evidence of cyclic strain hardening was observed in the tube that had not been pre-strained, and evidence of softening seen in the 10% and 20% pre-strained tubes. Macroscopic residual stresses were measured to be near zero at distances greater than 25 mm from the weld centre-line, but measurements in the 20% pre-strained tube revealed the presence of micro residual stresses having a magnitude of up to 50 MPa.

INTRODUCTION

The structural integrity, performance and life of weldments is determined by the mechanical properties of the weld metal, heat affected zone (HAZ) and parent materials. These properties depend on the full fabrication history including cold bending and swaging, welding, heat treatment and the effects of service ageing. For example, introduction of plastic strain can increase the susceptibility of materials to stress corrosion and creep damage [1,2]. It is important to quantify the initial material properties in weldments in order to understand and assess their influence on the life and integrity of components.

In this project, the separate and combined effects of manufacturing steps on austenitic stainless steel tube weldment properties at the room temperature were investigated. Effects of bending and swaging were simulated by plastically straining three identical stainless steel tubes to different levels (0%, 10% and 20%). Then each tube was cut into two halves and welded together. The aim of the work was to understand the combined effects of pre-straining and welding on the variation of mechanical properties and residual stress across the weldment. The variation in mechanical properties was measured using digital image correlation (DIC) and a series of strain gauges (SG). Residual stresses were measured on the 0% (undeformed) and 20% prestrained and welded tubes by using the neutron diffraction using the Stress-Spec instrument at the FRMII facility in Germany.

EXPERIMENTAL

Test specimens

A set of pre-strained and butt-welded tubes were supplied for the experimental programme by a power generation company (Table 1). The untreated tubes (before pre-straining and welding) were manufactured by extrusion and solution annealed at a temperature of 1100°C for 3 mins followed by water quenching. The tubing material is AISI Type 316H austenitic stainless steel with the composition given in Table 2. The initial tubing geometry was 38 mm in diameter and 4 mm in thickness. The test specimens were fabricated as follows. First two tubes were pulled uniaxially in tension up to 10 and 20% plastic strain (referred to as “pre-straining”). Secondly, these tubes plus a non-strained (0%) tube were each cut into two halves. Matching half-tubes were then welded together (after root tack welding) using a tungsten inert gas (TIG) welding process with Type 316L filler metal (see Tables 2 and 3).



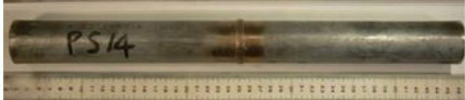
Pre-strained and welded tubes	Degree of plastic deformation	Label of tubes	Label of the remote-end tensile specimens	Label of the cross-weld tensile specimens
	0%	A ₀	B ₀	C ₀
	10%	A ₁₀	B ₁₀	C ₁₀
	20%	A ₂₀	B ₂₀	C ₂₀

Table 1: Photographs and labeling of test specimens

	Cr	Ni	Mo	Mn	Si	Co	C
316H	16.89	11.25	2.04	1.55	0.53	0.089	0.05
316L	18.38	12.07	2.53	1.61	0.37	-	0.01

Table 2: The composition of the stainless steel tubing material (Type 316H) and the weld material (Type 316L)

Welding Type	TIG
Polarity	DCEN (Direct current electrode negative)
Shield & Purge Gas	Argon 99.995%
Current	65-140 A
Flow Rate	5 to 8 litres/min
Electrode	2.4 mm 2% Th or Ce Tungsten
Purge Rate	2 to 8 litres/min

Table 3: Weld procedure specification

The welded tubes A₀ and A₂₀ were used for neutron diffraction residual stress measurements. Thereafter, flat cross-weld (C₀, C₁₀, C₂₀) and remote-end (B₀, B₁₀, B₂₀) tensile test specimens were cut from A₀, A₁₀ and A₂₀ tubes by electro-discharge machining. The cut position and the dimensions of the tensile specimens are given in Figure 1.

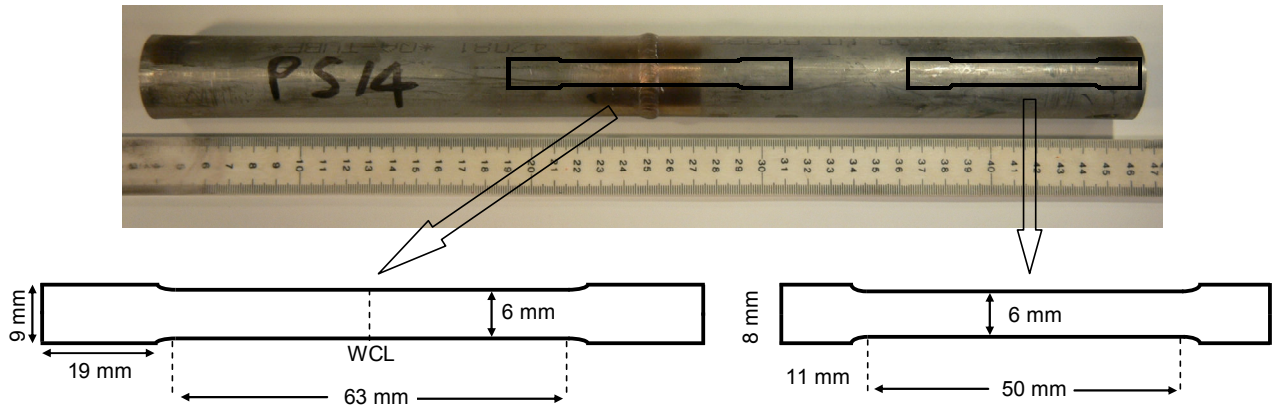


Figure 1: The cut position (top) and the dimensions of the cross-weld test specimens C_0 , C_{10} and C_{20} (bottom left) and tensile specimens B_0 , B_{10} and B_{20} (bottom right). Both types of specimen were 3mm thick.

Residual stress measurements using neutron diffraction

The Stress-Spec neutron diffraction instrument at the FRMII facility in Germany was used to determine the distribution of weld residual stresses in welded tubes A_0 and A_{20} . A wavelength of $\lambda = 1.5480 \text{ \AA}$ was obtained using a Si (400) monochromator. This wavelength allowed measurement of the austenitic steel (311) reflection at a scattering angle $2\theta_s \approx 91^\circ$. The gauge volume used in our measurements was $2 \times 2 \times 2 \text{ mm}^3$. For both tubes, the lattice strain response, ε_{lat} , in the axial, hoop and radial directions was measured at the mid-thickness along one half of the tubes with a position opposite to the start/stop point of the final weld pass, as shown in Figure 2. The measured data were analyzed with StressTexCalculator software using Gaussian fitting to obtain the peak positions in terms of 2θ angles which were then used to calculate the strain. Measurements at the remote end of welded tube A_0 in axial, hoop and radial directions were used as direction-dependent references (θ_0) to calculate the lattice strain for each measurement.

$$\varepsilon_{lat} = \frac{\Delta d}{d} = \frac{\sin \theta_0}{\sin \theta} - 1 \quad (1)$$

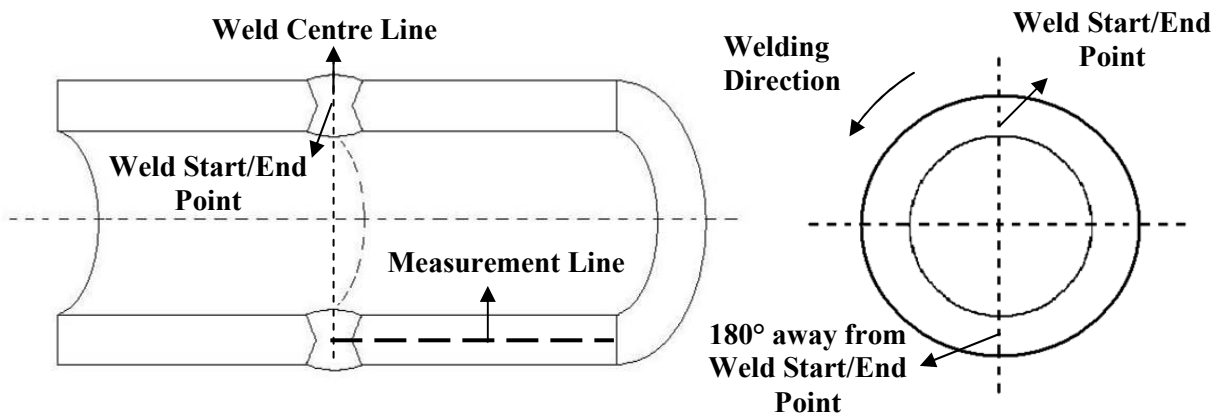


Figure 2: Sketch showing location of neutron diffraction measurement lines in specimens A_0 and A_{20}

The strain measured is in the direction of the scattering vector. To find out the stress state at any point in the sample, measurements are usually required in six orientations due to the fact that stress is a tensor. However, it was assumed that the principal stress axes coincide with the axial, hoop and radial directions of the tube [3]. Hence the stress in the principal directions can be calculated using the Hookes' law. For example, the stress in the axial direction was calculated using the following equation:

$$\sigma_{axial} = \frac{E}{(1+\nu)(1-2\nu)} \left[(1-\nu)\varepsilon_{axial} + \nu(\varepsilon_{hoop} + \varepsilon_{radial}) \right] \quad (2)$$

where crystallographic elastic constants for the (311) reflection were taken to be $E = 195$ GPa and $\nu = 0.29$.

Tensile tests and Digital Image Correlation

Tension tests on cross-weld specimens C_0 , C_{10} and C_{20} were carried out using a screw-driven tensile testing machine with a 30kN load cell. Mechanical wedge action grips were used to fix the specimens into the machine. Before each test commenced, the loading and specimen alignment was checked in order to avoid subjecting the specimen to any bending or torsion, i.e. to ensure the loading was pure uniaxial tension [4,5]. This was achieved by employing universal joints in the loading fixture, and checking the alignment with a pair of SGs attached on opposite faces of the specimen 20 mm away from the weld centre line (WCL), see Figure 3. Two more SGs were attached onto the back surface at the middle of the weld and in the HAZ (6.5 mm away from WCL). The data from these SGs were compared to the DIC results obtained from the area shown with dash rectangle in Figure 3.

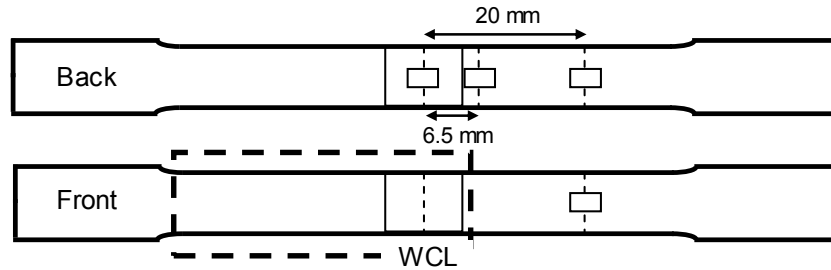


Figure 3: Positions of SGs on the back and front surfaces of specimens C_0 , C_{10} and C_{20}

The full field distribution of strain in the area shown in Figure 3 was obtained throughout each tensile test using DIC. The speckle pattern required for the DIC measurements was achieved by white light illumination of the rough surface produced by EDM [6]. After correcting the alignment of the specimen and grips, the tensile tests were performed with a constant extension rate of 0.1mm/min. During the tests, images of the front surface of the specimens were captured by a digital SLR camera (Nikon D300), with a sensor size of 4,288 x 2,848 pixels (12.3 Mega Pixels), and a 200 mm macro lens. A DC fibre optic light source was used to illuminate the surface. The images were taken every 10 seconds from the half-length of the specimen indicated in Figure 3 and the load and extension were recorded every second. Analysis of the images was performed using commercial DIC software [7].

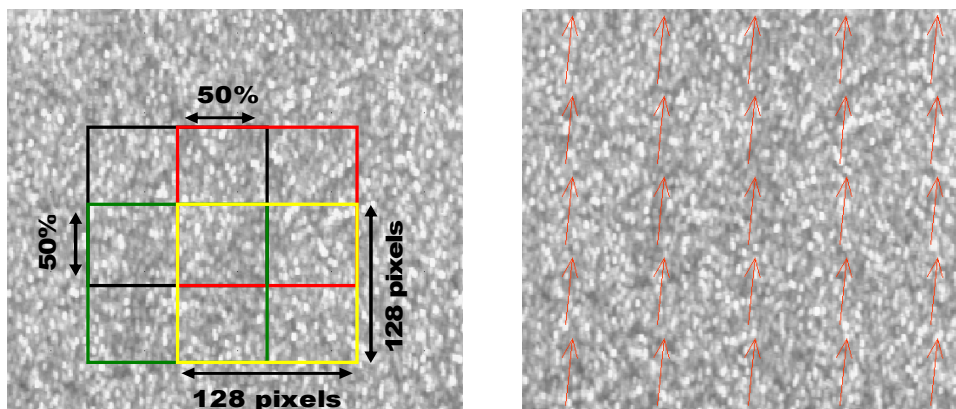


Figure 4: Reference image and the subsets used for the calculations (left) and the displacement vectors on the image of the deformed surface after 1190 sec (right)

All images from the three tension tests (of cross-weld specimens C_0 , C_{10} and C_{20}) were analyzed using the same optimized parameters as described in [6]. The pixel size on the real images for each test was about 11 μm . As a first step of analysis, all images were shift-corrected with respect to the reference image. Then, the displacement

vectors in the loading direction were calculated by multi-scanning the images using a '256x256 subset size with 50% overlap and 2 passes' and a '128x128 subset size with 50% overlap and 6 passes' respectively (Figure 4). After the displacement map in the loading direction was obtained using the DIC software, the strain was calculated by differentiating the displacement data using a Matlab script [6]. The error in the calculated strain is estimated to be about 50 microstrain; this is based on the precision of the DIC method which is given as 0.02 pixel displacement [7]. The strain on each image was averaged across the width of the specimen and a stress-strain curve was constructed for each subset. A linear line was fitted to the elastic region of each stress-strain curve and used to determine the 0.2% yield stress of the material.

RESULTS

Figure 5 illustrates tensile stress-strain curves for the parent material of tubes A_0 and A_{20} measured on specimens B_0 and B_{20} using an extensometer. These specimens were extracted from positions remote from the influence of the welds (see Figure 1). The 0.2% and 1% yield stress data derived from these curves are tabulated in Figure 5. The B_{20} curve superposes on the B_0 stress-strain curve if translated by 22.5% strain; this suggests that the A_0 tube must have been pre-strained slightly more than the 20% value reported by the supplier.

Stress-strain curves for cross-weld specimens C_0 , C_{10} and C_{20} at the weld centre obtained from SG and DIC measurements are given in Figure 6. Results from the two measurement techniques show a good correlation with each other for specimens C_{10} and C_{20} . Although the SG data for specimen C_0 suggest higher yield stress behaviour than measured by DIC it should be noted that these measurements were made on opposite sides of the test specimen. Overall the stress-strain properties of the weld metal in all three specimens are very similar to each other.

Stress-strain curves for cross-weld specimens C_0 , C_{10} and C_{20} at 6.5mm from the weld centre-line (WCL) obtained from SG and DIC measurements are given in Figure 7. Results from the two measurement techniques show a good correlation with each other for specimens C_0 and C_{10} . However, the DIC and SG stress-strain curves for specimen C_{20} deviate sharply from each other soon after first yield owing to necking of the weld metal (see discussion).

Stress-strain curves for cross-weld specimens C_0 , C_{10} and C_{20} at 10mm from the WCL obtained from DIC measurements are given in Figure 8. The sudden change in shape of the curves for specimens C_{10} and C_{20} at around 340 MPa is associated with necking of the weld metal (as indicated in Figure 8).

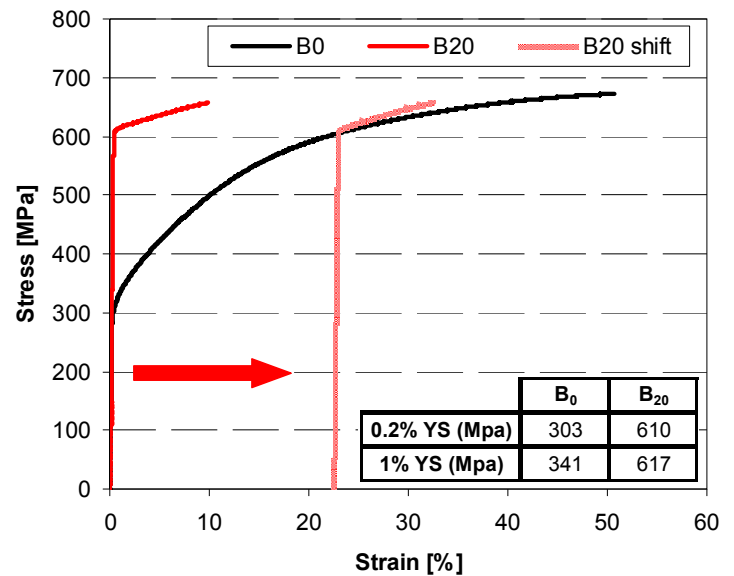


Figure 5: Stress-strain curves from specimens B_0 and B_{20} measured using a side extensometer

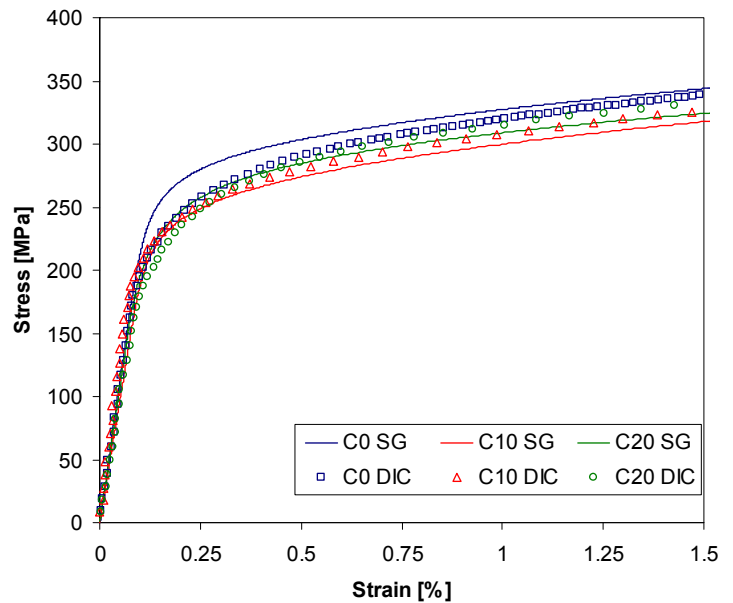


Figure 6: Stress-strain data measured using SG and DIC for the weld centre of test specimens C_0 , C_{10} , and C_{20}

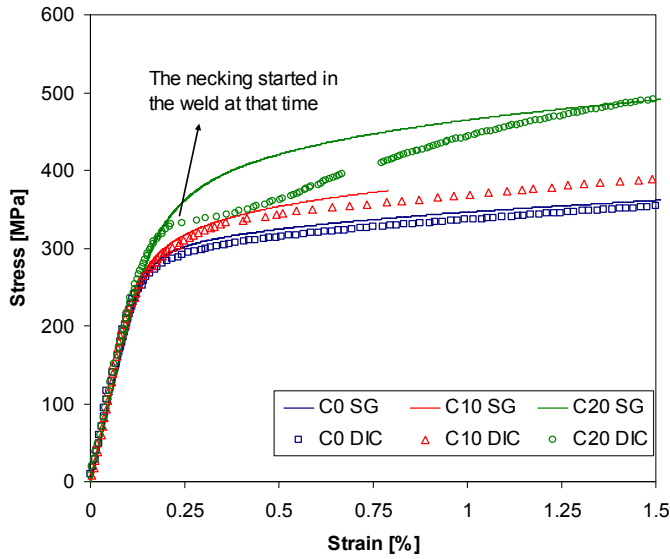


Figure 7: Stress-strain data measured using SG and DIC at 6.5mm from the WCL of test specimens C_0 , C_{10} , and C_{20} (the gap in C_{20} data at 0.7% strain is due to the connection problem between the camera and PC during the experiment and the SG on specimen C_{10} decohered after 0.8% strain)

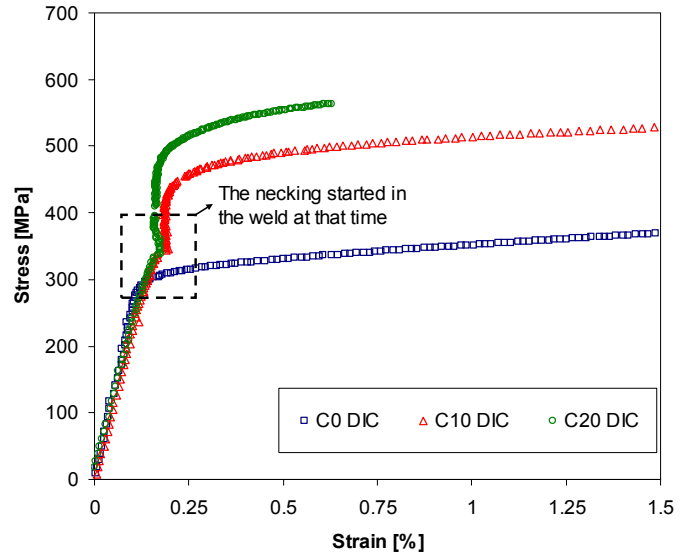


Figure 8: Stress-strain data measured using DIC at 10mm from the WCL of test specimens C_0 , C_{10} , and C_{20}

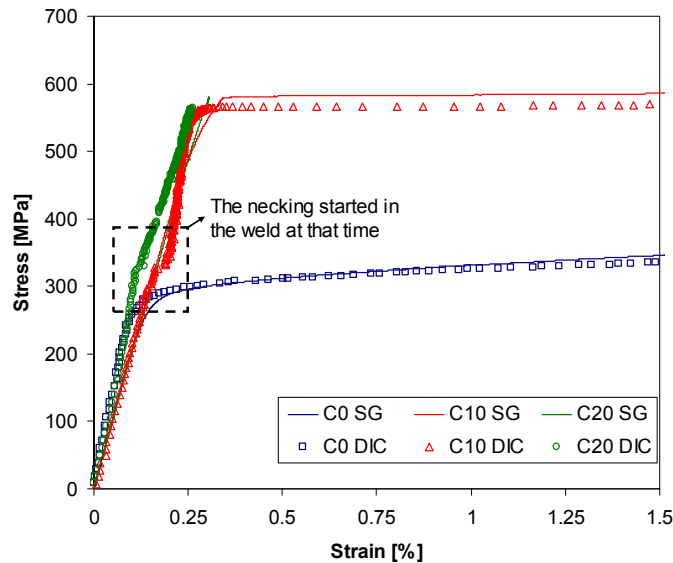


Figure 9: Stress-strain data measured using SGs and DIC at 20mm from the WCL of test specimens C_0 , C_{10} , and C_{20}

Stress-strain curves for cross-weld specimens C_0 , C_{10} and C_{20} at 10mm from the WCL obtained from SG and DIC measurements are given in Figure 9. The discontinuity in the shape of the curves for specimens C_{10} and C_{20} at around 340 MPa is again probably associated with necking of the weld metal (see Figures 7 and 8). But it is interesting that the SG data do not exhibit such a trend (see discussion).

Figure 10 plots the variation of 0.2% yield stress along the half-length of cross-weld specimens C_0 , C_{10} and C_{20} based on analysis of the DIC stress-strain curves. In specimen C_0 , the yield stress increases from a minimum of 268 MPa in the weld region to a maximum of 319 MPa at 10mm from the WCL and then drops gradually to a

steady value of 285 MPa at about 25mm from the WCL. In specimen C_{10} , the yield stress increases steadily from a minimum of 260 MPa in the weld region to a maximum of about 565 MPa at 16mm from the WCL. The trend in yield stress for specimen C_{20} is similar to C_{10} but in this case the yield stress is difficult to define because of necking behaviour of the weld metal.

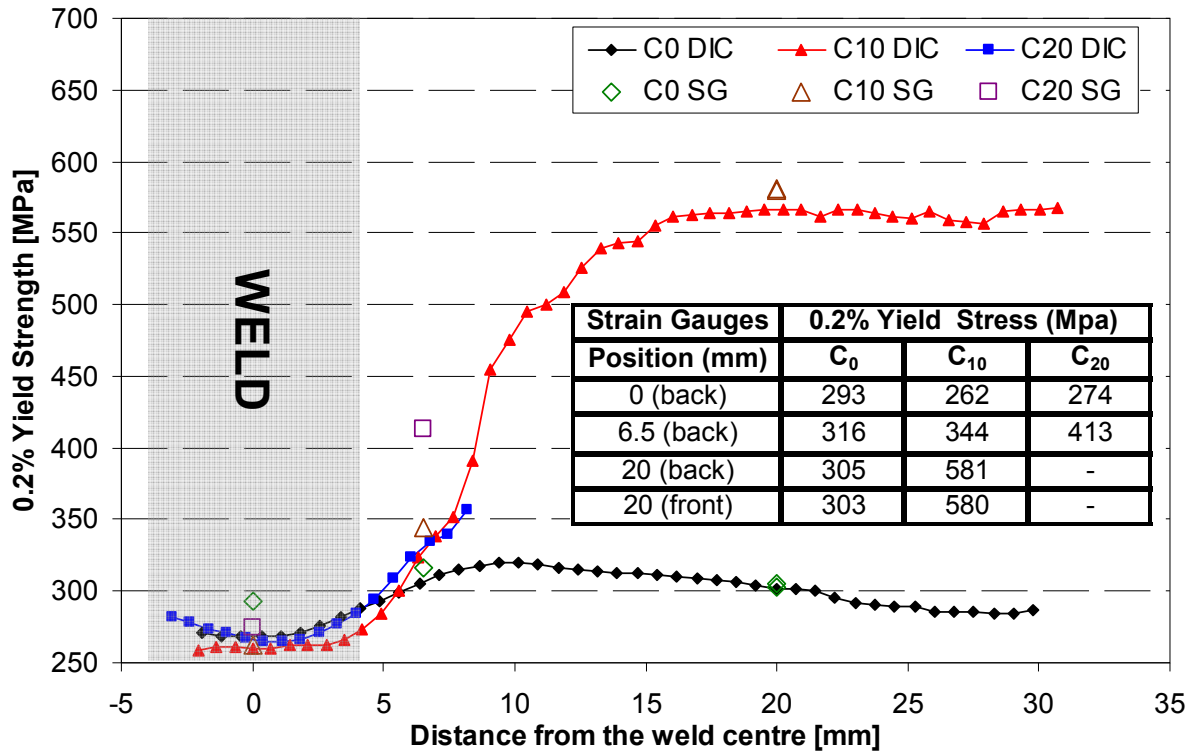


Figure 10: Variation in measured 0.2% yield stress moving away from the WCL test specimens C_0 , C_{10} , and C_{20} (derived from SG and DIC data).

The table in Figure 10 shows values of 0.2% yield stress obtained with the SGs at 0, 6.5 and 20mm away from the WCL for all cross-weld specimens (C_0 , C_{10} and C_{20}). The data are plotted with open symbols. It is seen that SG measurements show a reasonable correlation with the DIC results apart from the ones at the weld centre on specimen C_0 and at 6.5mm on C_{20} . The latter is 70 MPa higher than the DIC measurement at that point.

Figure 11 shows the distributions of axial, hoop and radial residual stresses measured at mid-radius of test specimens A_0 and A_{20} up to 60mm from the WCL. The results of particular relevance to this paper are in zone 2 (25 – 60mm from the WCL). In test specimen A_0 , the measured stresses in all three directions are almost zero. Whereas the average stresses in zone 2 of specimen A_{20} are 25 MPa, -15 MPa and -50 MPa in the axial, radial and hoop directions respectively. The differences in measured stress are indicative of micro-stresses caused by the 20% plastic prior deformation of material in specimen A_{20} remote from the influence of the weld.

DISCUSSION

The stress-strain curves measured using DIC and SGs are in reasonable overall agreement with each other (see figures 6, 7 and 9). The differences can be attributed to measurement position (Figure 3) and strain localization. Note that the DIC results were averaged over the respective gauge lengths of the SGs used.

At the WCL, strain was measured by a SG attached on the opposite face of the specimen to DIC observations. Small differences in the stress-strain curves (Figure 6) could be caused by slight misalignment during the tests or by real differences in weld metal properties. The small differences between the SG and DIC curves for the C_0 and C_{10} specimens at 6.5mm and 20mm (Figures 7 and 9 respectively) are unsurprising given that the SGs were located on the opposite face and at the opposite end of the specimens. The deviation in stress-strain behaviour for the specimen C_{20} (Figure 7) at about 0.2% strain was associated with necking of the weld metal. This

phenomenon also caused the discontinuities in the stress-strain curves of specimens C₁₀ and C₂₀ seen at 10mm and 20mm from the WCL (Figures 8 and 9). The weld metal was much weaker in these two specimens because the parent tubes were work hardened by pre-straining 10% and 20%.

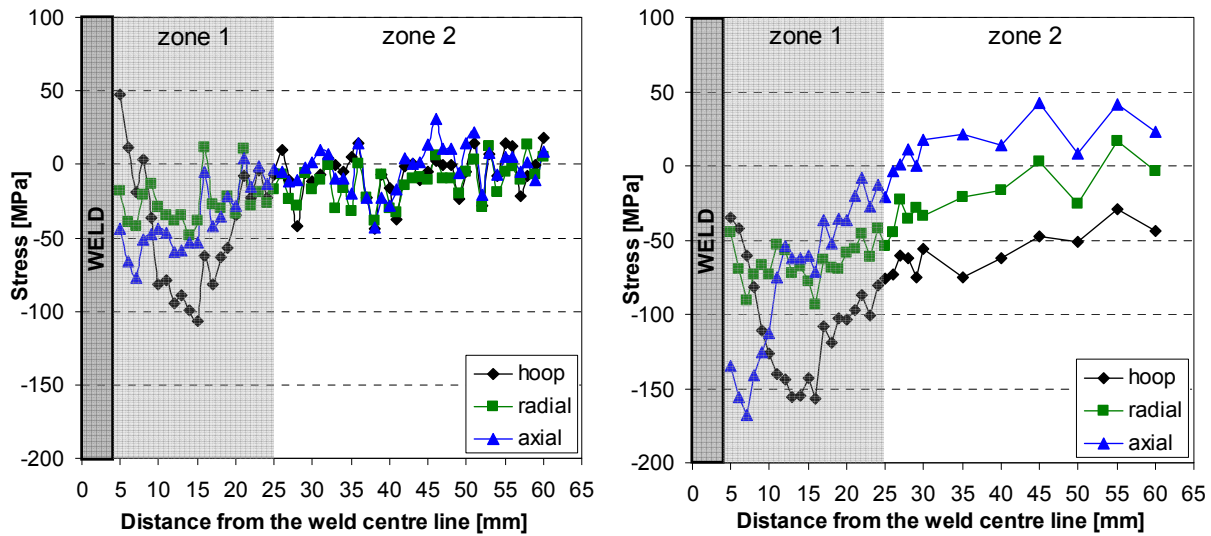


Figure 11: Variation in measured residual stress at mid-radius of test specimens A₀ (left) and A₂₀ (right) up to 60mm from the WCL. The Stress-tech neutron diffractometer at the FRMII facility (Munich) was used for the measurements (using the 311 reflection).

Pre-straining had a marked effect on the fracture behaviour of the specimens. The tensile test limits for C₀, C₁₀ and C₂₀ specimens were set to 15mm overall extension. Specimen C₀ didn't fail whereas C₁₀ and C₂₀ ruptured in the weld metal before they reached 10mm extension. In specimen C₀ the parent material yielded (0.2% yield stress of 285 – 303 MPa) and extended whereas the parent material of C₂₀ specimen was in elastic region (0.2% yield stress was 610 MPa, see Figure 5) when the specimen fractured.

The variation in 0.2% yield stress measured along the half-length of specimens C₀, C₁₀ and C₂₀ is given in figure 10. There is a very marked drop in yield stress in specimen C₁₀ approaching the weld from about 16mm away from the WCL. This is caused by the welding process. Parent material near the weld was heated to temperatures where creep (> 450°C) and dislocation annealing (>700°C) mechanisms operated.

The slight increase in yield stress of specimen C₀, in parent material between 5 and 25mm from the WCL is also associated with the welding process. But in this case the welding process has created strain hardening that has not entirely annealed out. The welding process introduces heat into adjacent parent material. This expands the material producing compressive residual stress of sufficient magnitude to initiate yielding. During cooling the region starts to contract and tensile strains develop. If the temperature gradient is high enough, this contraction can also yield the material in tension. Thus thermal cycles associated with welding can cause cyclic strain hardening in material adjacent to a weld. The extent of the yield zone in a thin welded plate can be estimated with the formula below [9]:

$$y_0 = \frac{1.033 K}{\sigma_{yp}} \cdot \frac{\eta q}{\nu t} \tag{3}$$

where y_0 = radius of yield zone, mm q = arc power, J/sec t = thickness, mm
 K = a material constant, Nmm/J η = process efficiency
 σ_{yp} = 0.2% yield stress, MPa ν = weld travel speed, mm/sec

This gives a yield length of 13.5 - 31 mm assuming a heat input of $q = 500 - 1100$ J/sec, $t = 4$ mm, $K\eta = 161$ Nmm/J, $\sigma_{yp} = 303$ MPa and $\nu = 5$ mm/sec. Adding this distance to the ½-width of the weld (4mm) gives a yield

distance of 15.5 - 33 mm from the WCL. This distance correlates with the yield stress distribution in specimen C₀ specimen shown in Figure 10.

The residual stresses measured by neutron diffraction (see Figure 11) show a complex variation approaching the weld (in zone 1); these results will be addressed in a future publication. The results of interest here are those in parent material unaffected by the welding process. Note the above results suggest that material further than 25mm away from the WCL is unaffected by hardening and softening mechanisms associated with welding. The residual stress measurements in zone 2 (25 – 60mm) of the non-pre-strained component, welded tube A₀, are close to zero in each direction. This confirms that material in this zone is unaffected by the weld. However, the average stresses in zone 2 of specimen A₂₀ are 25 MPa, -15 MPa and -50 MPa in the axial, radial and hoop directions respectively. The differences in measured stress are indicative of micro-stresses caused by 20% plastic prior deformation of material in specimen A₂₀ remote from the influence of the weld. In zone 1, the welding harshly alters the plastic strain which is already present in the material and that results in a very complicated strain distribution for different crystallographic planes [11].

CONCLUSIONS

1. The spatial variation in stress-strain behaviour across the weldment of plastically pre-strained welded tubes has been measured using DIC and conventional SGs and a reasonable agreement between the results obtained.
2. The DIC results were observed to be highly sensitive to deformation localization in the weld metal of the pre-strained sample.
3. The welding process had a marked effect on the tensile properties of parent material within 25mm of the weld centre-line. Evidence of cyclic strain hardening was observed in the tube that had not been pre-strained, and evidence of softening seen in the 10% and 20% pre-strained tubes.
4. Macroscopic residual stresses were measured to be near zero at distances greater than 25 mm from the weld centre-line, but measurements in the 20% pre-strained tube revealed the presence of micro residual stresses having a magnitude of up to 50 MPa.

ACKNOWLEDGEMENTS

The authors would like to thank British Energy Generation Limited for providing the welded tubes and funding the research. Professor Bouchard gratefully acknowledges Royal Society Industry Fellowship support. MEF is supported by a grant through The Open University from the Lloyd's Register Educational Trust, an independent charity working to achieve advances in transportation, science, engineering and technology education, training and research worldwide for the benefit of all.

REFERENCES

- [1] Willis M, McDonough-Smith A, Hales R, "Prestrain effects on creep ductility of a 316 stainless steel light forging" *International Journal of Pressure Vessels and Piping*, 76(6), 355-359 (1999)
- [2] Kamaya M, Wilkinson AJ, Titchmarsh JM "Quantification of plastic strain of stainless steel and nickel alloy by electron backscatter diffraction" *Acta Materialia*, 54(2), 539-548 (2006)
- [3] Hofmann M, Wimpory RC "NET TG1: Residual stress analysis on a single bead weld on a steel plate using neutron diffraction at the new engineering instrument STRESS-SPEC" *International Journal of Pressure Vessels and Piping*, 86(1), 122-125 (2009)
- [4] Christ BW, Swanson SR "Alignment Problems in the Tensile Test" *Journal of Testing and Evaluation (JTE)*, 4(6), 405-417 (1976)
- [5] Gray TGF, McCombe A "Influence of specimen dimension and grip in tensile testing steel to EN 10 002" *Ironmaking and Steelmaking*, 19(5), 402-408 (1992)
- [6] Acar M, Gungor S, Ganguly S, Bouchard PJ, Fitzpatrick ME, "Variation of Mechanical Properties in a Multi-pass Weld Measured Using Digital Image Correlation" *Proceedings of the SEM Annual Conference*, Albuquerque New Mexico USA Society for Experimental Mechanics Inc. (2009).
- [7] "StrainMaster 2D - Getting Started" *LaVision User Manual*.

- [8] Kotecki DJ, "Ferrite control in duplex stainless steel weld metal" *Weld. J.* 65 (10), 273-278 (1986).
- [9] Procedure R6 Revision 4. Assessment of the integrity of structures containing defects, Section IV.4, Gloucester, UK: British Energy Generation Ltd (2007).
- [10] Timoshenko SP, Woinowsky-Krieger "Theory of plates and shells" 2nd ed. New York, McGraw-Hill, 466-497 (1959).
- [11] Acar MO, Bouchard PJ, Fonseca JQ, Fitzpatrick ME, Gungor S "Intergranular Strains in Pre-Strained and Welded Pipes", *Material Science Forum*, 2009 (in press).